

Investigation of a three-phase thermochemical reactor through an experimentally validated numerical modelling

Zeng, C, Liu, S, Yang, L, Han, X, Song, M & Shukla, A

Author post-print (accepted) deposited by Coventry University's Repository

Original citation & hyperlink:

Zeng, C, Liu, S, Yang, L, Han, X, Song, M & Shukla, A 2019, 'Investigation of a three-phase thermochemical reactor through an experimentally validated numerical modelling', Applied Thermal Engineering, vol. 162, 114223.

<https://dx.doi.org/10.1016/j.applthermaleng.2019.114223>

DOI 10.1016/j.applthermaleng.2019.114223

ISSN 1359-4311

Publisher: Elsevier

NOTICE: this is the author's version of a work that was accepted for publication in , Applied Thermal Engineering. Changes resulting from the publishing process, such as peer review, editing, corrections, structural formatting, and other quality control mechanisms may not be reflected in this document. Changes may have been made to this work since it was submitted for publication. A definitive version was subsequently published in, Applied Thermal Engineering, [162] , (2019)] DOI: 10.1016/j.applthermaleng.2019.114223

© 2019, Elsevier. Licensed under the Creative Commons Attribution-NonCommercial-NoDerivatives 4.0 International

<http://creativecommons.org/licenses/by-nc-nd/4.0/10.1016/j.applthermaleng.2019.114223>

Copyright © and Moral Rights are retained by the author(s) and/ or other copyright owners. A copy can be downloaded for personal non-commercial research or study, without prior permission or charge. This item cannot be reproduced or quoted extensively from without first obtaining permission in writing from the copyright holder(s). The content must not be changed in any way or sold commercially in any format or medium without the formal permission of the copyright holders.

This document is the author's post-print version, incorporating any revisions agreed during the peer-review process. Some differences between the published version and this version may remain and you are advised to consult the published version if you wish to cite from it.

Investigation of a Three-phase Thermochemical Reactor through an Experimentally Validated Numerical Modelling

Cheng Zeng¹, Shuli Liu^{1*}, Liu Yang², Xiaojing Han², Ming Song², Ashish Shukla¹

¹Centre for Research in the Built and Natural Environment, Coventry University, Coventry CV1 2FB, UK

²School of Mechanical Engineering, Beijing Institute of Technology, China

*Corresponding author at: School of Energy, Construction and Environment, Coventry University, Coventry CV1 2FB, UK. Email: Shuli.Liu@coventry.ac.uk

Abstract

For some renewable energy such as solar energy, the mismatch between the side of generation and demand should be tackled by thermal energy storage techniques with high energy density and low thermal losses. Thermochemical energy storage is a promising technology to meet these requirements. Within a thermochemical energy storage system, reactor is one of the critical components to achieve the optimal performance. **While few studies have investigated the three-phase reactor applied in open thermochemical system in building's application.** This study presents a numerical description of a three-phase thermochemical reactor with air, solid thermochemical material and water flow. Zeolite 13X has been selected as the working thermochemical material and experimental tests have been conducted to obtain the temperature profiles in both the charging and discharging processes. **A two dimensional numerical model of the reactors has been developed, verified and validated. A good agreement has been obtained by comparing the numerical and experimental results with the root mean square percent error ranging from 6.02% to 12.29%. Additionally, parameters sensitivity analysis has been conducted for reference diffusivity, heterogeneity factor, and initial water uptake of the zeolite.** The numerical model and the investigation provide the tool reactor design optimisation, charging and discharging processes evaluation and reactor performance improvement.

Keywords: Thermochemical energy storage; Adsorption; Numerical modelling; Three-phase thermochemical reactor, Zeolite 13X

Nomenclature

<u>Symbol</u>	<u>Term</u>	<u>Unit</u>
A	contact area	m^2
A_1	adsorption potential	J/kg
a	specific surface area of adsorbent	m^2/m^3
c_p	specific heat capacity at constant pressure	J/(kg·K)
D	diameter	m
D_e	equivalent diffusivity of adsorbent particles	m^2/s
D_0	reference diffusivity of adsorbent particles	m^2/s
d_p	diameter of adsorbent particle	m
E	characteristic energy of adsorption in Dubinin–Astakhov equation	J/kg _{H2O}
E_a	activation energy in linear driving force model	J/mol
h_r	enthalpy of adsorption	J/kg _{H2O}
h	convection heat transfer coefficient	W/(m ² ·K)
K	permeability of adsorbent	m^2
k_m	mass transfer resistance coefficient in linear driving force model	1/s
L	length	m
m	mass	kg
\dot{m}	mass flow rate	kg/s
Nu	Nusselt number	-
n	heterogeneity parameter	-
P	pressure	Pa
Pr	Prandtl number	-
R	ideal gas constant	J/(K·mol)
Re	Reynolds number	-
R_w	specific gas constant of water vapour	J/(kg·K)
r_p	radius	m
r'	coefficient of correlation	-
T	temperature	K
t	time	s

U	thermal conductance	$W/(m^2 \cdot K)$
u	velocity	m/s
W	adsorption volume	$m^3/kg_{\text{adsorbent}}$
w	absolute humidity ratio of air	$kg_{H_2O}/kg_{\text{dry air}}$
X	water uptake of adsorbent	$kg_{H_2O}/kg_{\text{adsorbent}}$
Greek symbols		
α	thermal diffusivity	m^2/s
δ	metal pipe thickness	m
ε	porosity	-
ρ	density	kg/m^3
λ	thermal conductivity	$W/(m \cdot K)$
μ	dynamic viscosity	$Pa \cdot s$
ν	kinematic viscosity	m^2/s
Subscriptions and superscriptions		
0	reference point	
a	air	
b	reactor bed	
e	equilibrium	
in	inlet flow	
m	metal tube	
out	outlet flow	
p	zeolite particle	
s	dry adsorbent solid	
sat	saturation	
v	vapour	
w	water	

1. Introduction

To tackle climate and meet urgent energy conservation goals around the world, the application of renewable energy in buildings is essential. Research findings indicate that the building sector is responsible for more than 30% of worldwide carbon emissions [1]. However, to increase the use of renewable energy and reduce the dependency of fossil fuels, the mismatch between the renewable energy generation and demand of end users should be tackled [2]. Taking solar energy as an example, at the generation side, it can be stored by thermochemical energy storage systems at times when abundantly available. When it gets dark the energy can be released and provide a continuous flow of clean energy to meet the space heating demand.

Thermochemical energy storage involves the process of reversible physical and chemical interaction between a solid (thermochemical material) and a working fluid (such as water vapour) to store and release thermal energy. Due to the principle of thermochemical reactions, the technology features nearly zero energy loss and 2-10 times higher energy storage density compared to water [3].

A critical part of a thermochemical energy storage system is the reactor. It contains thermochemical material and provide the space where the energy storage and release processes take place. The reactor has been considered as one of the vital components to achieve the optimal performance in energy charging and discharging [4–6]. In the current literature, despite the applied thermochemical materials, the reactor can be classified as two-phase and three-phase reactor. The two-phase reactor contains the thermochemical material and the sorption pair/reactant such as air or vapour. **While the three-phase reactor is added with a second working fluid. The second working fluid is disconnected from the other two reaction phases, but it acts as heat exchange media to supply/extract heat to/from the reactor.**

1.1. The state-of-the-art of the numerical thermochemical reactor studies

The majority of the reactor studies have been focusing on two-phase reactors. **Within the scope, in 2016, Tatsidjodoung et al. have developed a one dimensional numerical model to investigate the charging and discharging performance of a zeolite 13X packed bed reactor [7].** Then the authors have validated the model by comparing its

results with the experimental tests and suggested the suitable mass transfer resistance coefficient to achieve the desirable agreement between numerical and experimental results. In another study published in 2018, Kuznik et al. have developed and validated a three-dimensional numerical model of a zeolite 13X reactor for building's application [8]. The model considers the zeolite and air as two phases in a reactor with their own temperature. Validation has been conducted with respect to experimental tests under different charging temperature (120 °C and 180 °C) and air flow rates (60 m³/h, 80 m³/h, and 90 m³/h). Additionally, in 2017, Gaeini et al. have developed a two dimensional model to investigate the flow, moisture and heat transfer in a pack bed reactor [9]. When validating the model, the authors have used pressure drop, air flow velocity and adsorbent temperature profile obtained in the experimental tests. Specifically, the concentration of adsorbed water in the packed bed has been compared with the results from MRI (Magnetic Resonance Imaging) experiments.

When it comes to three-phase reactor studies, most of the studies are limited to the closed system which is isolated from the ambient with a specific working pressure. In 2016, Fopah-Lele et al. have presented a numerical investigation study in a three-phase reactor, as shown in Figure 1 (a) [10]. The cylinder chamber contains thermochemical material MgCl₂. In a discharging process, the water vapour enters the chamber at the bottom for heat release. A pipe fin heat exchanger is integrated in the chamber where heat transfer fluid such as water can travel through it for domestic hot water or space heating supply. Using the Comsol software, the authors have reported the results from an analytical sharp front model to identify the optimal parameters in order to achieve the desirable reactor performance. With a similar reactor design, in 2015, Schreiber et al. have reported a dynamic model to investigate the energy storage process of a closed thermochemical system for heat supply in industrial batch processes (Figure 1 (b)) [11]. To allow the heat transfer fluid temperature higher than 100 °C, thermal oil has been used as the working fluid in the heat exchanger. In another study, as shown in Figure 2 [12], a three-phase thermochemical reactor has been proposed and investigated numerically. The reactor is in sandwich structure where zeolite is integrated with heating/cooling panels at the top and bottom. The authors have built a three dimensional numerical model to evaluate the reactor geometrical configuration influences in the reactor performance. As reported by the authors, the model has been validated experimentally. Apart from integrating a heat

exchanger with the thermochemical material, some studies such as [13] and [14] have used air to oil heat exchanger at the air flow path to extract heat from the exhaust air. According to the experimental and numerical study in [14], the authors have reported that 60% of the released thermal power has been transferred to the working fluid while the other has been lost due to the insufficient heat insulation.

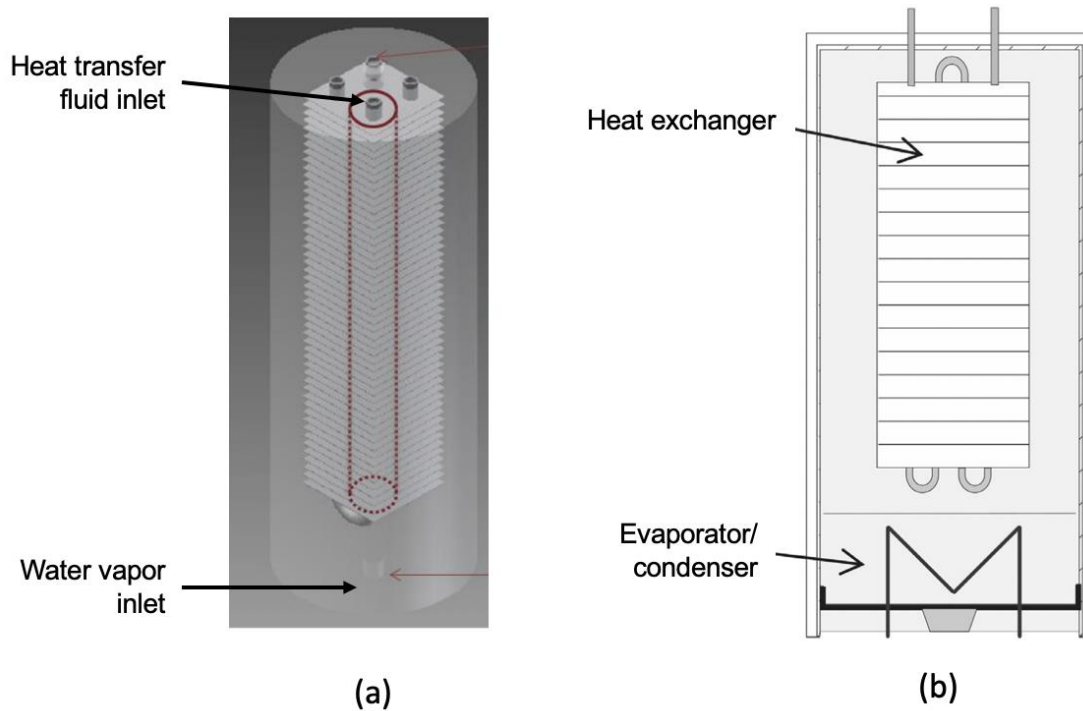


Figure 1 Three-phase thermochemical reactor: (a) Fin pipe exchanger in building's application [10], (b) heat exchanger for cogeneration in industrial batch process [11]

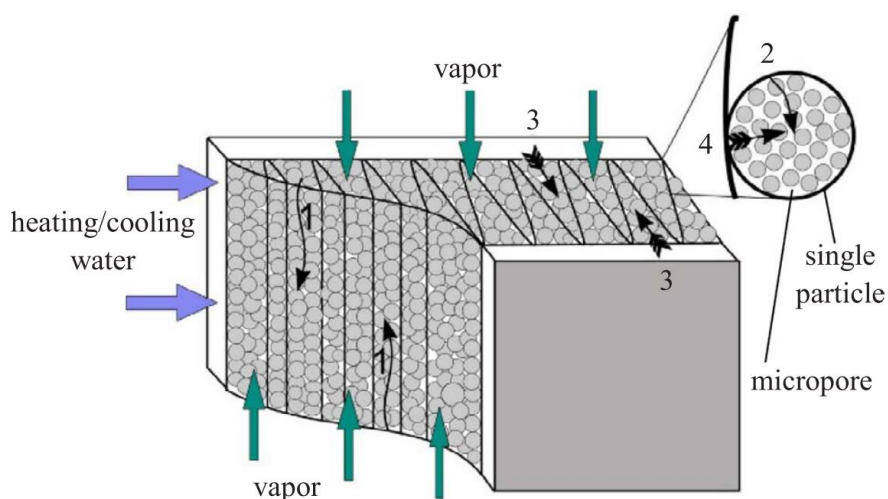


Figure 2 Cross section view of the sandwich structure three-phase reactor [12]

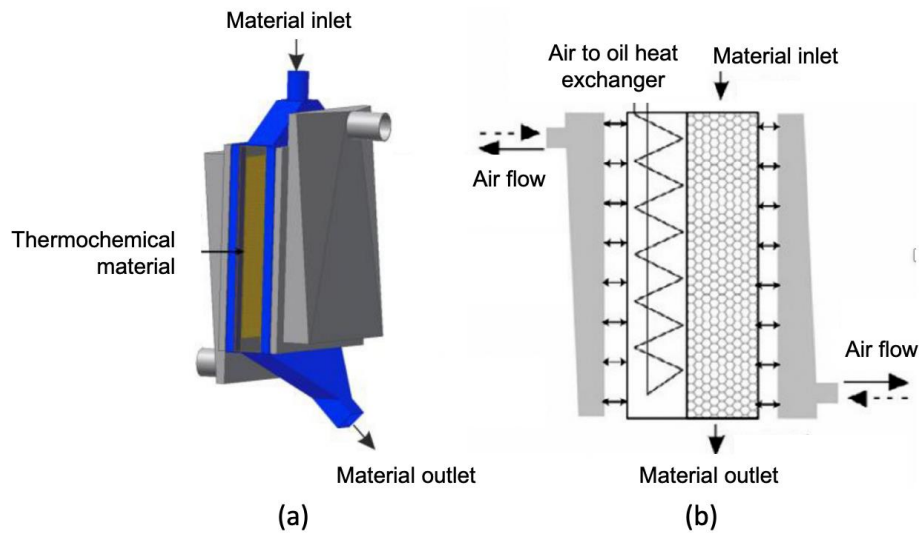


Figure 3 Heat exchanger located at the air flow path in a thermochemical reactor: (a) 3D illustration, (b) cross section view [14]

1.2. Aim and contributions of the paper

When reviewing these studies, currently, few studies have investigated the three-phase reactor applied in open thermochemical energy storage system. This paper aims to investigate a three-phase thermochemical reactor through an experimentally validated numerical model. A two dimensional thermochemical reactor numerical model has been developed and validated. The validation is supported by the original experimental data. The study methodology including reactor design, experimental setup and operation conditions are detailed in section 2. Section 3 describes the numerical model and section 4 presents the model verification and validation. Additionally, sensitive parameters affecting the reactor performance has been evaluated and presented. This paper provides a valuable approach for reactor performance analysis, reactor design optimisation, and performance improvement.

2. Methodology

The methodology of this study has been shown in Figure 4. The methodology section demonstrates the experimental system, experiment operation conditions, and statistical analysis indicators. The following section 3 details the reactor numerical modelling.

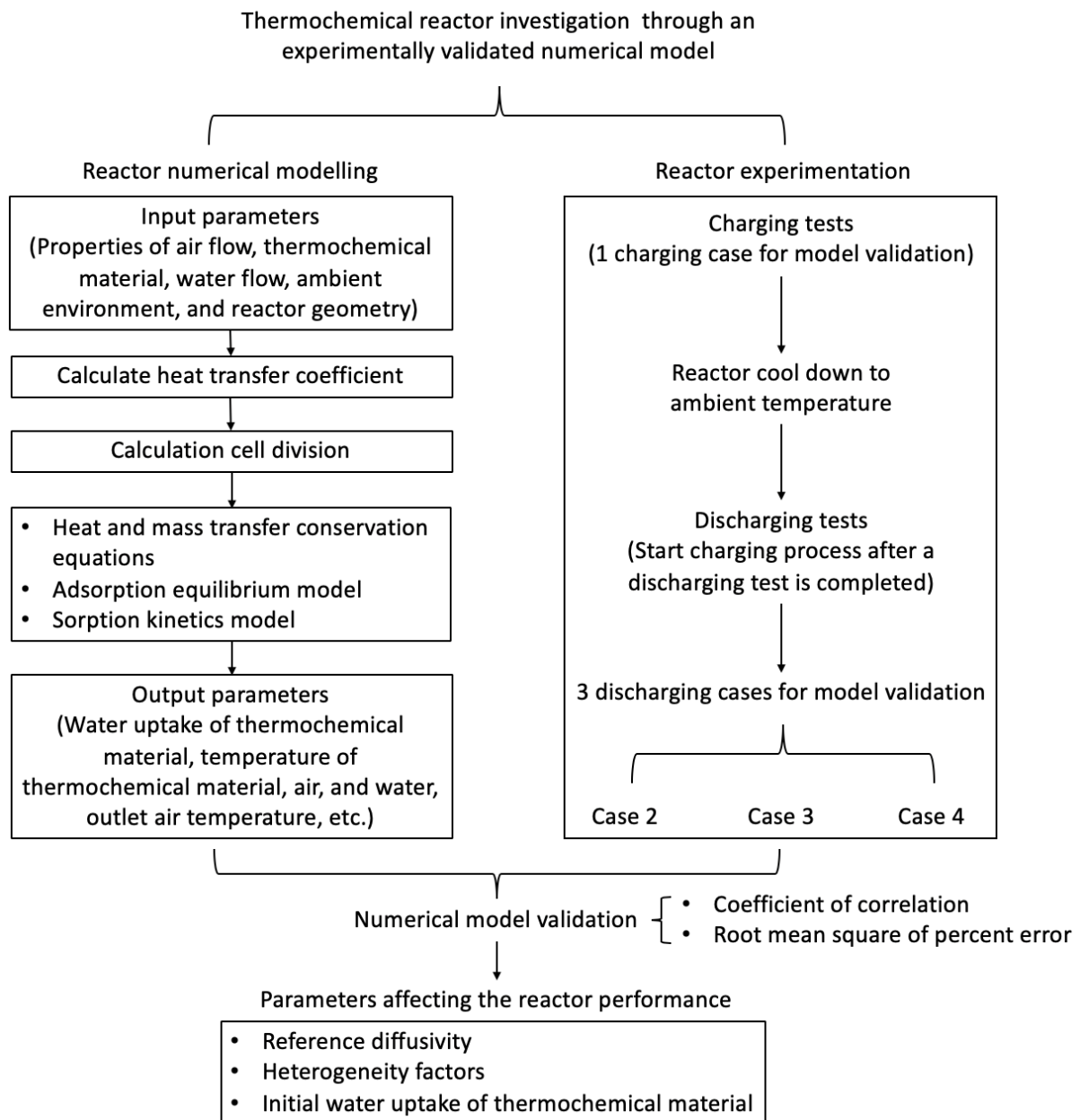


Figure 4 Graphic flow chart of the study methodology

In order to provide experimental results for the numerical model validation, an experimental system has been developed (Figure 5). In this system, an electric heater has been used to in charging processes. In discharging processes, water is the working fluid. Specifically, air from the ambient is pumped by the fan and driven through the platform. Firstly, it travels across the heat exchanger where the ambient air can be heated by the exhaust air. Then it travels through the air duct heater with 15 kW power and the ability 300 °C maximum outlet temperature. Next to the heater, a humidification pipe has been installed to connect the humidifier and the main air duct. The air can be humidified with the humidification capacity at 6 kg/h. Upon the

reactor entrance, the air flow is directed into the reactor. When the air leaving the reactors, it heads to the air to air heat exchanger where the sensible heat of the exhaust air transfer to the intake air from the ambient. With respect to the metal pipes, driven by a pump, water flows through the reactor and circulates to a water tank. In order to reduce the heat loss to the ambient and eliminate condensation across the air duct, the complete testing platform has been insulated using 50 mm thickness glass wool.

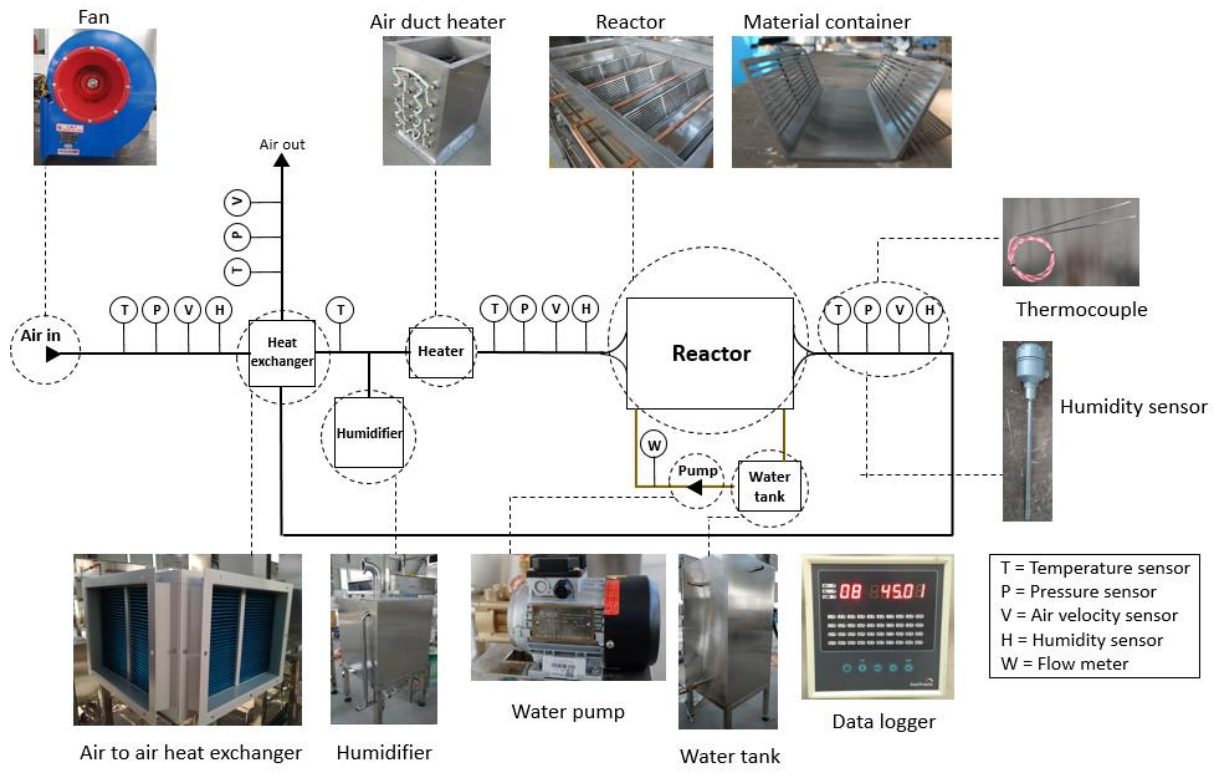


Figure 5 Schematic diagram of the experimental setup

Specifically, Figure 6 presents illustrations of the reactor container and pictures of the built reactor. Multiple side openings have been created as the air flow entrance and exit path. The width of the opening is 4 mm and the distance between any two openings is 3 mm. For the side of a built container, the openings are separated into three disconnected sections with separation bars to ensure accuracy of the opening geometry and structure stability during experimental tests. The distance between any two disconnected openings is 5 mm.

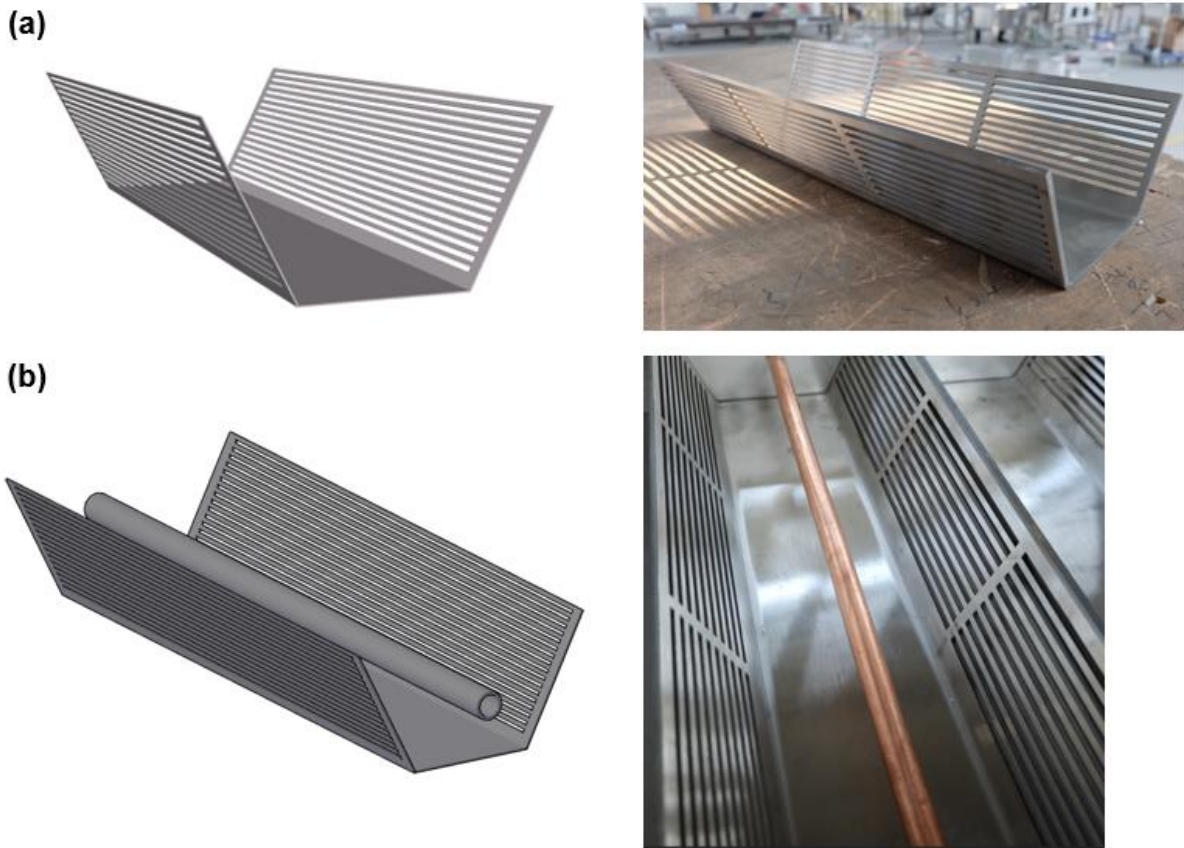


Figure 6 Illustrations of the reactor container and built reactor: (a) the container only, (b) the container with metal pipe installed

The numerical model is validated by comparing the modelling data with the experimental results. Four comparison cases are conducted in the validation. The operating conditions for the obtained experiment data are presented in Table 1. A set of charging experimental data (Case 1) and three sets of discharging data (Case 2, 3 and 4) have been used for the model validation. With respect to the discharging data, Case 2 is the discharging with humidified ambient; Case 3 is the discharging with humidified and preheated air at 50 °C; Case 4 is the discharging under the conditions of Case 3 but it turns on water circulation when reactor achieves peak temperature.

Table 1 Operating conditions for charging and discharging the reactor

Parameter	Unit	Discharging			
		Charging	Case 1	Case 2	Case 3
Ambient temperature	°C	21.33	18.52	13.21	21.18
Air flow rate	kg/s	0.048	0.024	0.045	0.045

Charging inlet temperature	°C	110	-	-	-
Discharging inlet temperature		-	18.52	50	50
Duration	hour	7	2	7	2
Water flow rate	L/min	-	-	-	0.5

When validating the numerical model by the experimental results, correlation between the numerical and experimental data is presented with coefficient of correlation. It measures how well the two sets of data are related and can be calculated with the following equation:

$$r' = \frac{N \sum_{i=1}^{i=N} F_i O_i - \sum_{i=1}^{i=N} (F_i) \sum_{i=1}^{i=N} (O_i)}{\sqrt{N \sum_{i=1}^{i=N} F_i^2 - (\sum_{i=1}^{i=N} F_i)^2} \sqrt{N \sum_{i=1}^{i=N} O_i^2 - (\sum_{i=1}^{i=N} O_i)^2}} \quad (1)$$

When there are N observations and forecast data, F_i represents one of the forecast data obtained from the numerical model, O_i represents an observed experimental data.

Additionally, the root mean square of percent error (RMSPE) has been applied to the model validation which measures the percentage difference between the forecast data and observed values, given in the following expression:

$$RMSPE = \sqrt{\frac{1}{N} \sum_{i=1}^{i=N} \left(\frac{O_i - F_i}{O_i} \right)^2} \times 100 \quad (2)$$

3. Reactor numerical modelling

3.1. Calculation method

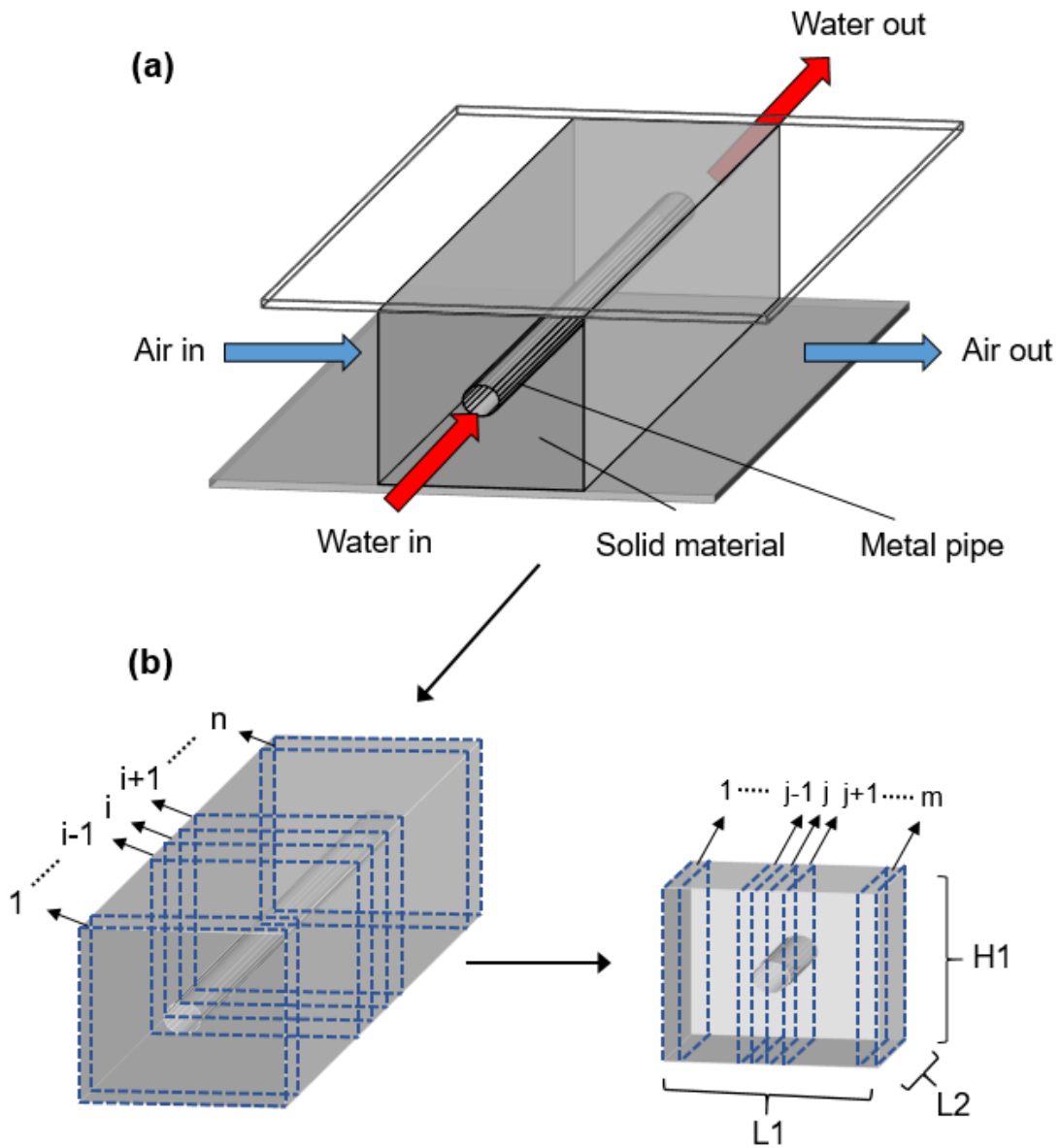


Figure 7 Illustration of the calculation method

Figure 7 illustrates the calculation method of the three-phase reactor model. It is consisted with air flow, water flow and solid thermochemical material. "Finite element" is used to transfer the reactor into numerous "differential" divisions where equations of heat and mass balance are applied to each element. As presented in Figure 7 (b), the whole calculation can be assumed to be integrated with unlimited elements with respect to the water flow direction, such as $i-1$, i , and $i+1$. Then to take the air flow into consideration, the computational element is further divided into sub-elements, such as

the $j-1$, j , and $j+1$. Newton iteration is used to achieve the equilibrium state of heat and mass transfer process.

With respect to the heat transfer within the reactor, it is induced by temperature difference of water, air flow, and solid adsorbent. For instance, if the water temperature is higher than the adsorbent and air, heat is transferred from water to the adsorbent and air flow, as presented in Figure 8. Additionally, when there is temperature difference between air flow and adsorbent, the heat transfer between the two are considered.

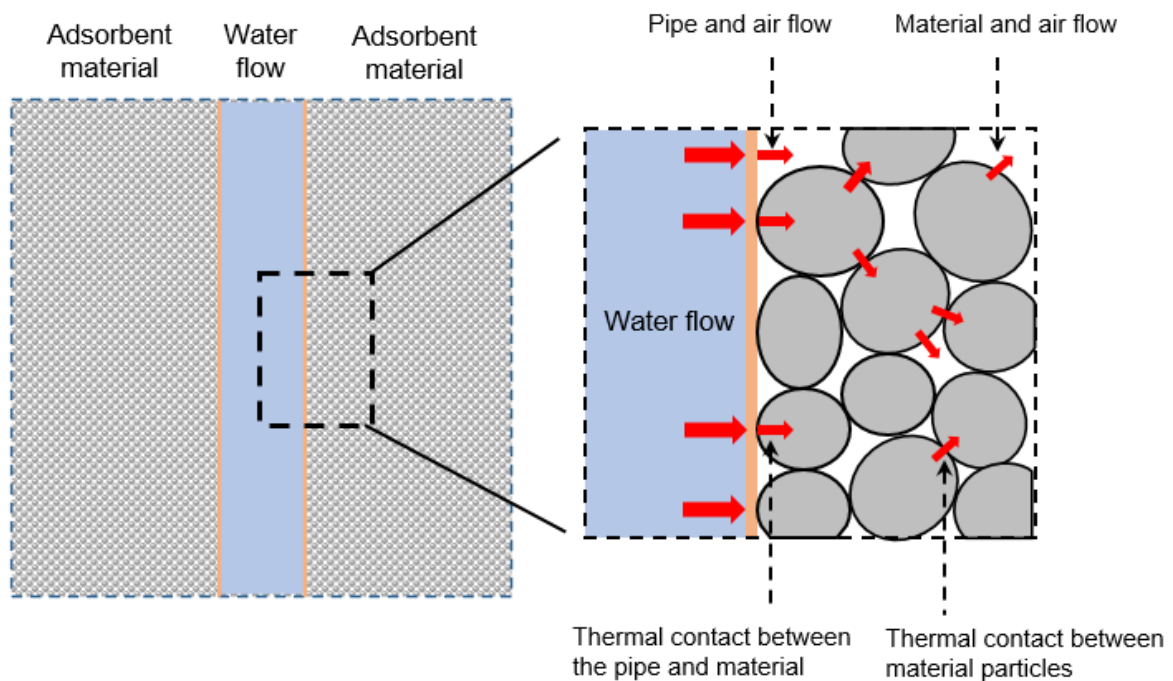


Figure 8 Heat transfer details in a porous bed with metal pipe

To simplify the numerical simulation process, the following assumptions have been made:

- Zeolite particles share the same property in the reactor and a unique bed porosity is used in the model [7];
- Physical properties of zeolite such as thermal conductivity and specific heat capacity are not varying with temperature;
- Radiative heat transfer, conductive heat transfer between adsorbent particles, work done by pressure changes, and viscous dissipation are neglected;
- The humid air is assumed to be ideal gas with the composition of dry air and vapour;

- The external wall of the reactor is assumed adiabatic.

3.2. Heat and mass transfer conservation equations

Table 2 summaries the heat and mass transfer conservation equations in the thermochemical reactor. Heat transfer between air and zeolite, air and water, and water and zeolite have been presented. Some specific considerations are illustrated as follow.

In terms of the convective heat transfer coefficient $h_{s,a} = 1/R_{conv}$ for solid adsorbent and air. It depends on the adsorbent particle diameter and air flow velocity. With respect to the bed porosity ranging from 0.2 to 0.9, Kuwahara et al. have proposed a correlation which has been reported to agree well with the experiment data [15]. The correlation has been given in equation (3). Considering the relatively wider application range of bed porosity, this correlation is used in the present study.

$$\frac{h_{s,a}d_p}{\lambda_a} = \left(1 + \frac{4(1 - \varepsilon_b)}{\varepsilon_b}\right) + \frac{1}{2}(1 - \varepsilon_b)^{1/2}Re^{0.6}Pr^{1/3} \quad (3)$$

The convective heat transfer resistance can be obtained and written in equation (4).

$$R_{conv} = \frac{1}{h_{s,a}} = \frac{d_p}{\lambda_a \left(\left(1 + \frac{4(1 - \varepsilon_b)}{\varepsilon_b}\right) + \frac{1}{2}(1 - \varepsilon_b)^{1/2}Re^{0.6}Pr^{1/3} \right)} \quad (4)$$

With respect to the heat transfer between air and water flow, conductive thermal resistance of the metal pipe has been neglected. The terms of $h_{w,m}$ and $h_{m,a}$ are the heat transfer coefficient of water flow within the metal pipe and heat transfer coefficient of air flow across the metal pipe. They can be evaluated by their Nusselt number.

Nusselt number of water flow

The equations for calculating the Nusselt number of water flow is determined by whether it is laminar flow or turbulent flow. To identify the status, the critical Reynolds number is 2300. In terms of laminar flow, Sieder and Tate have given the equation according to their experimental data [16], expressed as:

$$Nu_w = 1.86 \left(Pe \frac{D}{L} \right)^{1/3} \left(\frac{\mu_w}{\mu_m} \right)^{0.14} \quad (5)$$

Where the Peclet Number Pe can be calculated with the Reynolds and Prandtl number.

$$Pe = RePr \quad (6)$$

When the water flow is turbulent flow, the Nusselt number can be calculated by the equation proposed by Dittus and Boelter [16], expressed as:

$$Nu_w = 0.023Re^{0.8}Pr^n \text{ with } \begin{cases} n = 0.3 \text{ for charging the adsorbent} \\ n = 0.4 \text{ for discharging the adsorbent} \end{cases} \quad (7)$$

Where the Reynolds, Prandtl and Nusselt number is referred as:

$$Re = \left(\frac{uD}{\nu} \right)_w \quad (8)$$

$$Pr = \left(\frac{\mu c_p}{\lambda} \right)_w \quad (9)$$

$$Nu_w = \left(\frac{hD}{\lambda} \right)_w \quad (10)$$

Nusselt number of air flow through the metal pipe

Considering air flowing over the metal pipe embedded in porous medium, the Nusselt number can be expressed as [17]:

$$Nu_D = 1.015(RePr)_D^{1/2} \quad (11)$$

Therefore, the convective heat transfer coefficient $h_{m,a}$ can be calculated with equation (12).

$$h_{m,a} = \frac{\lambda_a \cdot 1.015 \left(\frac{\rho_a u_a D c_{p,a}}{\lambda_a} \right)^{1/2}}{D} \quad (12)$$

Additionally, the contact area of metal pipe and adsorbent particle is:

$$dA_{m,s} = (1 - \varepsilon_b) \cdot \pi D \cdot L_2 \quad (13)$$

Table 2 Summary of the heat and mass transfer equations in the numerical model

Terms	Equations
Heat transfer between zeolite and air	
Convective heat transfer between solid adsorbent and air flow	$\underbrace{\frac{dq_{s \rightarrow a}}{\text{Heat transfer rate}}}_{\text{Heat transfer from zeolite to air}} = \underbrace{(T_s - T_{a,in}) / \left(\frac{1}{U_{s,a}}\right) dA_{s,a}}_{\text{Heat transfer from zeolite to air}}$
Overall conductance $U_{s,a}$ for heat conduction within a zeolite particle and heat convection between the adsorbent particle and air flow	$\frac{1}{U_{s,a}} = R_{conv} + R_{cond}$
Conductive heat transfer resistance within the adsorbent particle [18]	$R_{cond} = \frac{d_p}{2\lambda_b} \left(1 - \frac{1}{\sqrt[3]{2}}\right)$
Convective heat transfer resistance [15]	$R_{conv} = \frac{1}{h_{s,a}} = \frac{d_p}{\lambda_a \left(\left(1 + \frac{4(1 - \varepsilon_b)}{\varepsilon_b}\right) + \frac{1}{2}(1 - \varepsilon_b)^{1/2} Re^{0.6} Pr^{1/3} \right)}$
Heat transfer between air and water flow	
Heat transfer rate of air and water flow	$dq_{a \rightarrow w} = (T_{a,in} - T_{w,in}) / \left(\frac{1}{h_{w,m} \cdot dA_w} + \frac{1}{h_{m,a} \cdot dA_{m,a}} \right)$
Heat transfer coefficient of water flow	$h_{w,m} = 0.023\lambda_w \left(\frac{uD}{\nu}\right)_w^{0.8} \left(\frac{\mu c_p}{\lambda}\right)_w^n \text{ with } \begin{cases} n = 0.3 \text{ for charging the adsorbent} \\ n = 0.4 \text{ for discharging the adsorbent} \end{cases}$

Heat transfer coefficient of air flowing over metal pipe

$$h_{m,a} = \frac{\lambda_a \cdot 1.015 \left(\frac{\rho_a u_a D c_{p,a}}{\lambda_a} \right)^{1/2}}{D}$$

Heat transfer between water and zeolite

Conductive heat transfer between metal pipe and zeolite

$$dq_{w \rightarrow solid} = (T_{w,in} - T_s) / \left(\frac{1}{h_{w,m} \cdot dA_w} \right)$$

Mass transfer between zeolite and air

Mass balance

$$\underbrace{\dot{m}_a (w_{a,out} - w_{a,in})}_{\text{Change of mass for air}} = \underbrace{-\frac{dX}{dt} m_s}_{\text{Change of mass for zeolite}}$$

3.3. Numerical model of adsorption equilibrium and sorption kinetics

Equilibrium and kinetics are two basic ingredients of adsorption and desorption processes. Equilibrium data provide information about initial and final state of a system while kinetics offer the change of chemical properties in time especially the rate of change. This section illustrates the applied equations for zeolite/water equilibrium and adsorption/desorption kinetics.

3.3.1. Zeolite and water equilibrium

The zeolite's water mass fraction equilibrium, i.e. isotherm, is calculated using the Dubinin-Astakhov equation, given in equation (14) [19]. W_0 is to maximum adsorption volume of the microporous system; and W is the volume which has been filled by the water molecules.

$$W = W_0 \exp \left[- \left(\frac{A_1}{E} \right)^n \right] \quad (14)$$

An essential parameter is A_1 , defined by:

$$A_1 = R_w T \ln \left(\frac{P_{sat}}{P_v} \right) \quad (15)$$

By Polanyi, A_1 is the adsorption potential. In this equation, P_v is the equilibrium pressure at temperature T ; P_{sat} is the saturated vapour pressure which can be expressed by [20]:

$$P_{sat} = 0.61121 \exp \left(\left(18.678 - \frac{T}{234.5} \right) \left(\frac{T}{257.14 + T} \right) \right) \quad (16)$$

It is noted that the unit in the P_{sat} equation is kPa for P_{sat} and °C for T .

Dubinin and co-workers considered the adsorption process to be a process of volume filling and introduced the ratio W/W_0 as the degree of filling of the micropores. Additionally, they adopted a thermodynamic interpretation from Polanyi adsorption potential and conducted a fundamental postulate that $W/W_0 = f(A/E)$. Dubinin and Astakhov expanded the equation with the addition of a parameter n , then simplified to the Dubinin-Astakhov equation. Additionally, Mette et al. have validated the Dubinin-Astakhov equation by comparing with the results from experimental measurements [21]. The authors have confirmed the applicability of the equation and suggested the corresponding values of the parameters are: $W_0 = 0.341e^{-3} \text{ m}^3/\text{kg}$, $E = 1.1923e6 \text{ J/kg}$.

Once obtained the volume of the adsorption water molecules W , the related water uptake (mass ratio of the adsorbed water) can be calculated. The water uptake at equilibrium state is calculated using the density of the adsorbed moisture ρ_{H_2O} and adsorption volume W .

$$X_e = \rho_{H_2O} \cdot W \quad (17)$$

$$\rho_{H_2O} = \frac{\rho_{20C}}{1 + \beta_{20C}(T_s - 293.15)} \quad (18)$$

Where ρ_{20C} is the moisture density at 20 °C and β_{20C} is the thermal expansion coefficient of water vapour at 20 °C.

The term n is referred as the heterogeneity factor. In general, heterogeneity is observed when adsorbed molecules display varying affinity to the adsorbent surface depending on the surface location [22]. Due to the nature of matter, there are always shoulders, peaks and valleys on the adsorbent material. These shoulders, peaks and valleys can be non-uniform chemical composition, surface defects, porosity, etc. The heterogeneity factor reflects the width of energy distribution [23]. This parameter is further analysed in the parameter sensitivity analysis section.

3.3.2. Mass transfer resistance using linear driving force model

Mass transfer resistance occurs when moisture transfers between its fluid phases to micro-pores of adsorbent. To describe the mass transfer resistance, linear driving force model can be applied. The model, originally proposed by Glueckauf and Coates (1947), has been frequently used because it is simple and analytical [25]. The linear driving force model gives the rate of water uptake in equation (19).

$$\frac{dX}{dt} = k_m(X_e - X) \quad (19)$$

where X_e is the equilibrium water uptake of adsorbent at time t in terms of air vapour pressure P_v and adsorbent temperature T ; however, X is the actual water uptake of the adsorbent at time t . The other coefficient k_m is the internal mass transfer coefficient. It is obtained from experimental data [26] with a function of adsorbent particle radius r_p and diffusivity D_e .

$$k_m = 15 \frac{D_e}{r_p^2} \quad (20)$$

The equivalent diffusivity can be expressed as [18]:

$$D_e = D_0 \exp\left(-\frac{E_a}{RT_s}\right) \quad (21)$$

3.4. Differential heat of adsorption

Thanks to the sorption mechanism and air flow, the energy transferred to the zeolite leads to the removal of water. The energy stored in the zeolite can be calculated by the multiplication of the change of enthalpy of adsorption h_r and change of water uptake. In this model, a polynomial fitting approximation of the measured heat of adsorption from Figure 9 [27] is used to determine the heat of adsorption at water uptake of X . The correlation between the differential enthalpy of adsorption h_r and zeolite water uptake X is expressed as:

$$h_r = 7 \times 10^7 X^6 - 7 \times 10^7 X^5 + 3 \times 10^7 X^4 - 7 \times 10^6 X^3 + 899951 X^2 - 69983 X + 6491.3 \quad (22)$$

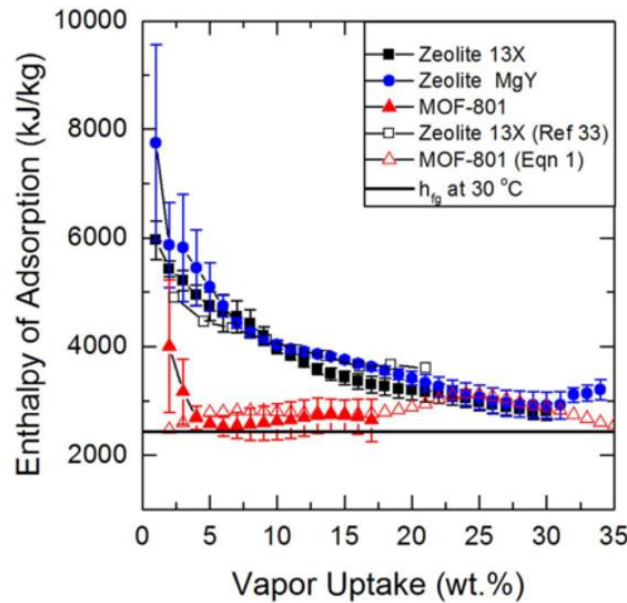


Figure 9 Adsorption enthalpy as function of water uptake (latent heat of evaporation 2430 kJ/kg at 30 °C) [27]

3.5. Viscosity of air

The viscosity of air μ represents its resistance to shearing flows. However, it is dynamic since the value for air at 180 °C is 40% higher than that of 20 °C. Therefore, its dependence to air temperature cannot be assumed to be negligible. The correlation in equation (23) has been used to calculate the air dynamic viscosity [8].

$$\mu(T_a) = 4.564 \times 10^{-8} \times T_a + 4.745 \times 10^{-6} \quad (23)$$

3.6. Effective air flow velocity

The velocity of humid air through the adsorbent bed is determined by Darcy's equation [28].

$$\vec{u}_a = -\frac{K}{\mu} \vec{grad}(P) \quad (24)$$

Where K is the permeability of the adsorbent bed. It given by the hydraulic radius theory of Carman-Kozeny relation as follow equation (25) [28]:

$$K = \frac{d_p^2 \varepsilon_b^3}{180(1 - \varepsilon_b)^2} \quad (25)$$

Where d_p is the average zeolite particle diameter.

3.7. Simulation parameters

Parameters used in the simulation are given in Table 3.

Table 3 Parameters used in the numerical analysis

Parameter	Symbol	Value	Unit	Reference
Bed porosity	ε_b	0.39	-	[7]
Bead conductivity	λ_b	0.20	W/(m·K)	
Zeolite density	ρ_s	0.85e3	kg/m ³	
Activation energy	E_a	2.95e4	J/mol	
Reference diffusivity	D_0	2e-6	m ² /s	
Maximum adsorption volume	W_0	0.34e-3	m ³ /kg _{adsorbent}	[21]
Characteristic energy of adsorption in Dubinin–Astakhov equation	E	1.1923e6	J/kg _{H2O}	
Zeolite particle diameter	d_p	4.0e-3	m	[29]
Particle Porosity	ε_p	0.32	-	[30]
Dry air density	ρ_a	1.177	kg/m ³	[16]
Air thermal conductivity	λ_a	2.62e-2	W/(m·K)	

4. Results and discussions

By using the software Matlab, the equations in the numerical model has been solved. This section illustrates the model verification, validation, and sensitivity analysis of critical parameters.

4.1. Numerical model verification

Verification is conducted to determine and ensure the numerical model implementation accurately represents the conceptual description of the thermochemical reactor. Two approaches have been used in the verification process: static testing and dynamic testing [31].

In the static testing, the Matlab program has been carefully reviewed and bugs have been fixed. Specifically, the authors have walked through the sections of parameter input, calculation cell division, heat and mass transfer coefficient calculation, adsorption equilibrium, adsorption kinetics, heat and mass balance equations, and calculation output.

In the dynamic testing, the results of the numerical model have been compared with the simulation study by Tatsidjodoung et al. [7] in France, as shown in Table 4. Tatsidjodoung et al. have demonstrated the numerical model accuracy and applicability in their study. The parameters used by Tatsidjodoung et al. have been input to the current numerical model. For discharging simulation processes, two air inlet air flow velocity (0.06 m/s and 0.14 m/s) and two initial water uptake values (0.03 kg_{H2O}/kg_{zeolite} and 0.06 kg_{H2O}/kg_{zeolite}) have been used. The peak reactor outlet air temperature has been calculated with the current numerical model and compared with the results from Tatsidjodoung et al. [7]. It is noted that the results are good accordance with each other, showing robustness and reliability of the present numerical model.

Table 4 Comparison between present study results and simulation results

Study	Inlet air temperature (°C)	Inlet air flow velocity (m/s)	Zeolite mass (kg)	Initial water uptake (kg _{H2O} /kg _{zeolite})	Peak reactor outlet air temperature (°C)
Simulation [7]	20	0.06	40	0.03	57.4
	20	0.14	40	0.06	56.5
Present study	20	0.06	40	0.03	54.4
	20	0.14	40	0.06	52.6

4.2. Numerical model validation

To illustrate the degree of which the numerical model represents the actual world for the intended applicability, numerical model validation is conducted. This section compares the computed results with the experimental values in charging and discharging cases. The reactor outlet temperature, inlet air temperature and water outlet temperature are presented. For both of the experimental and numerical results, during the charging process, the Zeolite 13X temperature at the outlet side presents the reactor outlet temperature; while during the discharging stage, the reactor outlet temperature is the outlet air temperature.

4.2.1. Charging tests – Case 1

Figure 10 shows a comparison between the experimental and numerical results for the reactor outlet temperature during a 7-hour charging study. The discrepancy between the experimental and numerical results is seen when the temperature is rising to the charging inlet temperature. The maximum temperature discrepancy during this stage reaches at 25 °C. However, after the reactor outlet temperature increases to 72 °C, a good agreement is obtained. The temperature discrepancy can be resulted from:

- Heat loss from the reactor to the environment has not been considered in the numerical model
- Initial water content of zeolite in the charging test has not been identified. The difference in initial water content leads to different adsorption kinetics in the linear driving force model.

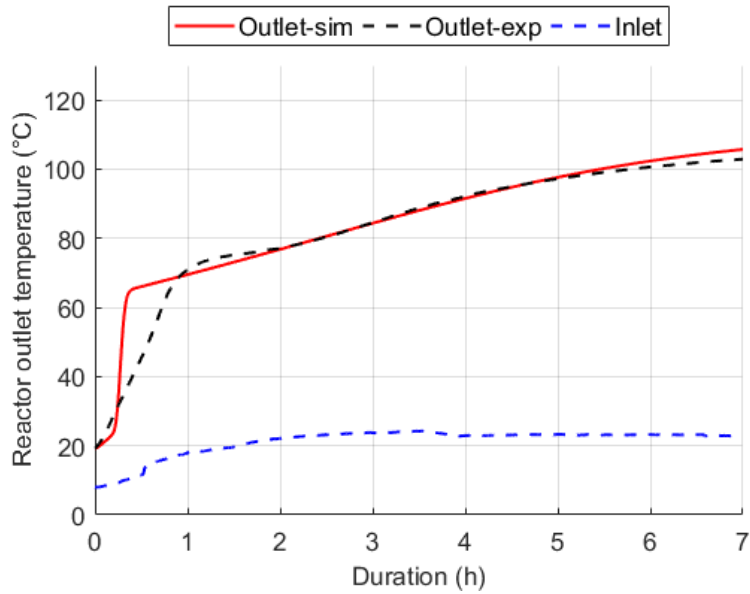


Figure 10 Measured and simulated inlet and outlet temperature of the reactor during the charging process

4.3. Discharging tests – Case 2 and 3

With respect to discharging, the comparison between computing values and experimental measurements are presented in Figure 11. Figure 11 (a) is the case 2 where zeolite 13X has been discharged with air at ambient temperature while Figure 11 (b) is for discharging with preheated air at 50 °C. Both figures have shown a good agreement between the experimental and numerical results. While for the numerical data, the reactor outlet temperature tends to achieve the peak discharging temperature faster than the values obtained in the experiment. The maximum temperature discrepancy has been observed during the temperature rising stage at 8 °C and 7 °C, respectively. Specifically, in Figure 11 (b), the temperature profile presents a noticeable difference for the discharging after 4.3 hours. Because the air duct heater has been switched off after 4.3 hours. In experimental tests, the residual heat from the heater continues to preheat the air. While in the numerical model, the transitional stage has not been considered.

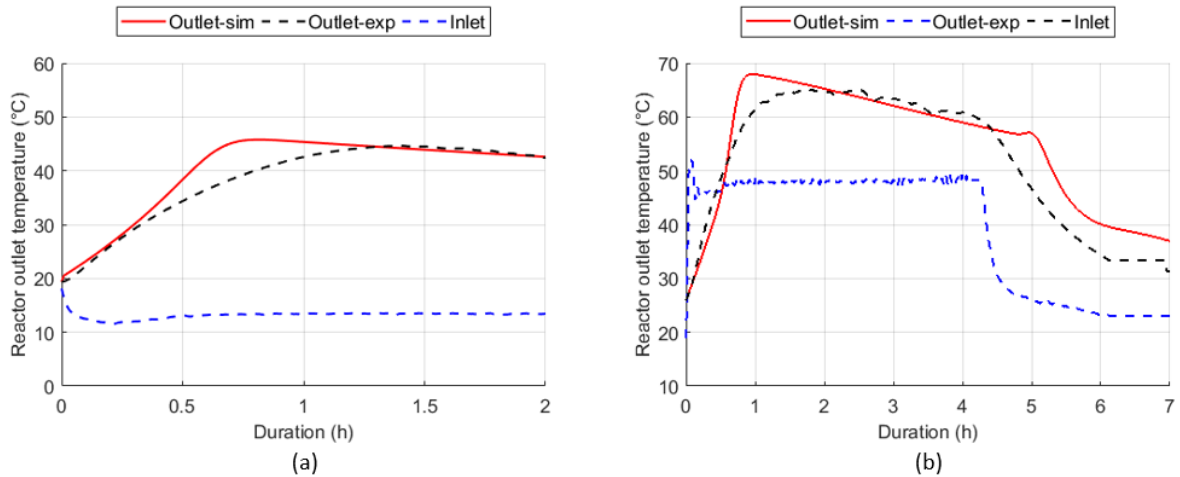


Figure 11 Measured and simulated reactor outlet temperature during the discharging process with (a) ambient air and (b) heated air

4.4. Discharging test – Case 4

Under the conditions of Case 3, water circulation has been switched on when the zeolite temperature reaches to the peak value at 68 °C. Figure 12 illustrates the comparison between the measured and computing values of water temperature at inlet and outlet of the reactor. An unstable temperature profile in the measurement has been witnessed. Because the heat from zeolite has been transferred to the metal pipe and water before 0.55 hours when the water circulation has been switched off. The transitional stage in the experiment has not been taken into validation. After this stage, the water circulation pump has been switched on and the inlet and outlet temperature profile become stable at 25 °C and 30 °C respectively. When comparing the experimental data with the computing values, the maximum temperature difference is 9.6 °C during 0.6 to 0.8 hours when the measurements is reducing to a relatively stable value at around 30 °C. After 0.8 hours, the temperature discrepancy drops to 1.1°C. The contributions to the discrepancy can be:

- The metal pipe energy accumulation has not been considered in the numerical model.
- In the experiment, thermocouples are attached to the outside of the metal pipe. Therefore, the measured pipe temperature has been considered as the water temperature.

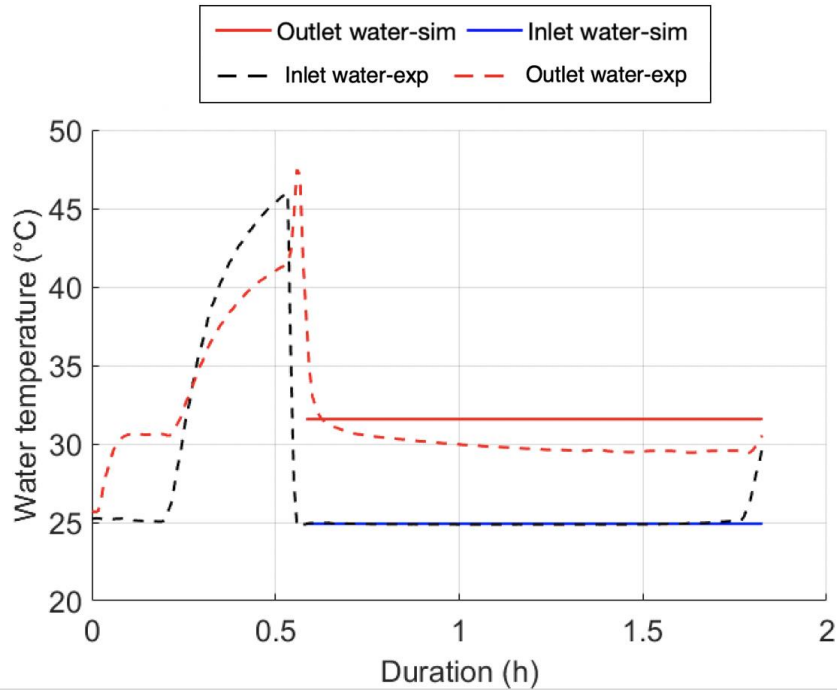


Figure 12 Measured and simulated inlet and outlet temperature of water

4.5. Statistical analysis results

The numerical model has been validated by comparing the computing values with the experimental results. Detailed statistical analysis is given in Table 5. The values of coefficient of correlation and root mean square percentage error have been calculated for validating the model for the three-phase thermochemical reactor. The maximum root mean square percent error is for Case 1 at 12.29%. As reported in literature, the acceptable error is 14% [32,33] or the average error of less than 12% [34]. Therefore, there is a good agreement between the computed and measured results in both the charging and discharging process.

Table 5 Statistical analysis

Parameter	Value			
	Charging		Discharging	
	Case 1	Case 2	Case 3	Case 4
Coefficient of correlation	0.96	0.94	0.95	-
Root mean square percent error (RMSPE)	12.29%	7.64%	10.53%	6.02%

4.6. Parameters sensitivity analysis

Three parameters have been identified as sensible on the reactor outlet temperature profile, the reference diffusivity D_0 , heterogeneity factor n , and initial water uptake X_0 . These parameters are critical to adsorption isotherm and adsorption kinetics which then affect the amount of heat charged or discharged from the thermochemical material. Additionally, however, literatures have reported uncertainty for the parameters. For instance, in terms of the heterogeneity factor, in general, value of $n < 2$ are for heterogeneous carbons and value of $n > 2$ are for highly homogeneous carbons. However, in [35], the suggested approximate value for zeolites is 4 to 6. While other literatures suggest the value ranges from 0.5 to 2 [36]. With respect to the reference diffusivity D_0 , variations can occur with different calculation method [25] and molar fraction [37]. For the initial water uptake, different experiment tests may start from different initial water uptake, affecting the adsorption kinetics and energy exchange scenario. This section presents how these parameters influence the reactor temperature profiles.

4.6.1. Effect of reference diffusivity (D_0)

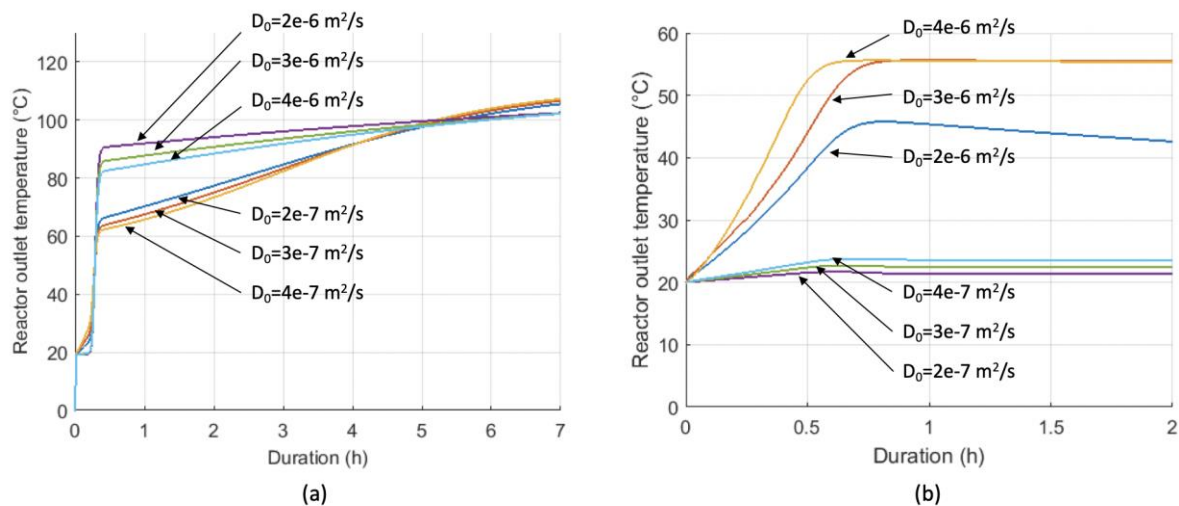


Figure 13 Influence of reference diffusivity to the temperature profile in (a) charging and (b) discharging

In charging, as shown in Figure 13 (a), the reference diffusivity influences the elevation of temperature profile with the respect to charging time. Relatively larger reference diffusivity reduces the time required for the reactor reaching the charging inlet temperature. With the charging duration from 0 to 1 hour, the reactor outlet

temperature increases to 80 °C ~ 95 °C for diffusivity from $2e-6 \text{ m}^2/\text{s}$ to $4e-6 \text{ m}^2/\text{s}$ while it increases to around 60 °C for diffusivity from $2e-7 \text{ m}^2/\text{s}$ to $4e-7 \text{ m}^2/\text{s}$. In discharging, as shown in Figure 13 (b), reference diffusivity ranging from $2e-7 \text{ m}^2/\text{s}$ to $4e-7 \text{ m}^2/\text{s}$ leads to less than 5 °C increase in reactor outlet temperature. While when the diffusivity increases to $2e-6 \text{ m}^2/\text{s}$ ~ $4e-6 \text{ m}^2/\text{s}$, the reactor temperature outlet increases significantly. Additionally, the steepness of the temperature profiles has been influenced by the diffusivity. According to the linear driving force model, the mass transfer coefficient increases with the rise of diffusivity. Therefore, relatively larger amount of adsorption energy has released, increasing the reactor outlet temperature.

4.6.2. Effect of heterogeneity factor (n)

Different heterogeneity factors for zeolite 13X have been reported in literatures [35,36]. The results presented below illustrate the effect of heterogeneity factor to the reactor outlet temperature (Figure 14). The heterogeneity factor n has been investigated from 0.5 to 6. At the beginning of the charging duration, there is a steep lift in the temperature profiles. The steepness has been enhanced by the increase of heterogeneity factor. At relatively larger heterogeneity factor, the reactor outlet temperature reaches to the heat source temperature in a reduced amount of time. In terms of discharging, heterogeneity factor affects the level of peak outlet temperature and the slope of the temperature profiles.

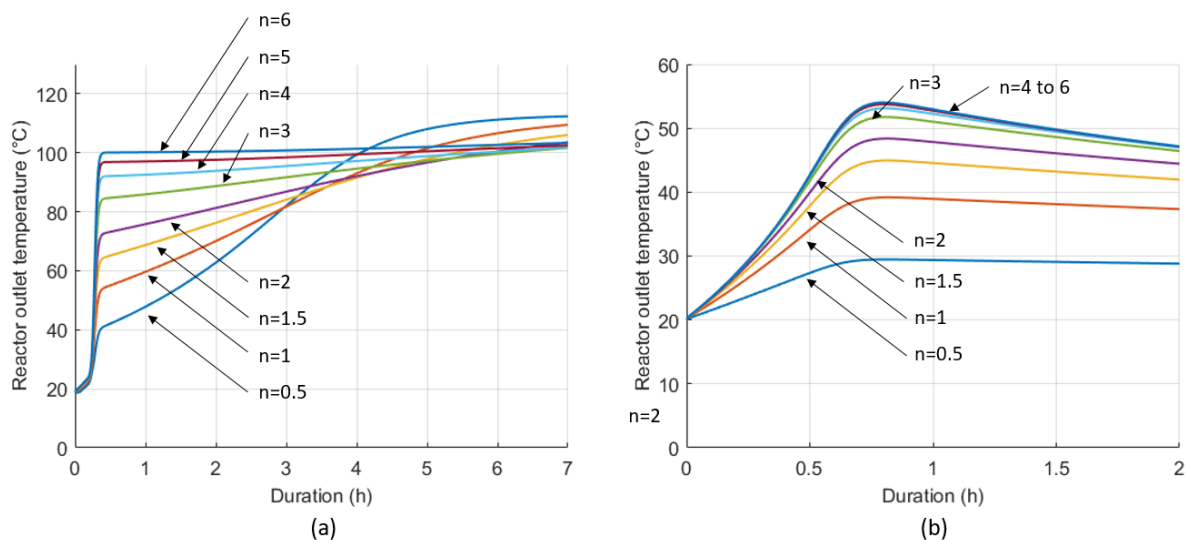


Figure 14 Influence of heterogeneity factor to the temperature profile in (a) charging and (b) discharging

4.6.3. Effect of initial water uptake (X_0)

The effect of initial water uptake of zeolite 13X has been evaluated, as shown in Figure 15. In terms of in charging, the relatively smaller initial water uptake increases the steepness of the outlet temperature profile and leads to a relatively higher temperature level within the first hour of charging. Within the duration, the margins among the reached temperature levels are reducing. However, when the initial water uptake is larger than $0.20 \text{ kg}_{\text{H}_2\text{O}}/\text{kg}_{\text{zeolite}}$, the outlet temperature profile starts dropping significantly in the first hour of charging. With the charging duration goes up to the hour of 7, all temperature profiles increase to the target charging temperature. Therefore, the initial water uptake is critical for the reactor temperature increasing at the start of a charging process. With respect to discharging, however, the relatively larger initial water uptake reduces the reactor outlet temperature drastically from around $55 \text{ }^\circ\text{C}$ to less than $20 \text{ }^\circ\text{C}$ (identical to the ambient temperature), as shown in Figure 15 (b). The initial water uptake at $0.15 \text{ kg}_{\text{H}_2\text{O}}/\text{kg}_{\text{zeolite}}$ can reach the peak discharging temperature under the current simulation conditions. The straight temperature profile indicates the adsorption energy is continuously transferring to the reactor within the 2 hours discharging session. However, when the initial water uptake increases to $0.30 \text{ kg}_{\text{H}_2\text{O}}/\text{kg}_{\text{zeolite}}$, the temperature profile has been reaching to the ambient temperature, indicating little adsorption energy release. Therefore, under the current simulation conditions, the initial water uptake at $0.20 \text{ kg}_{\text{H}_2\text{O}}/\text{kg}_{\text{zeolite}}$ is a critical value for the reactor to reach an optimal outlet temperature.

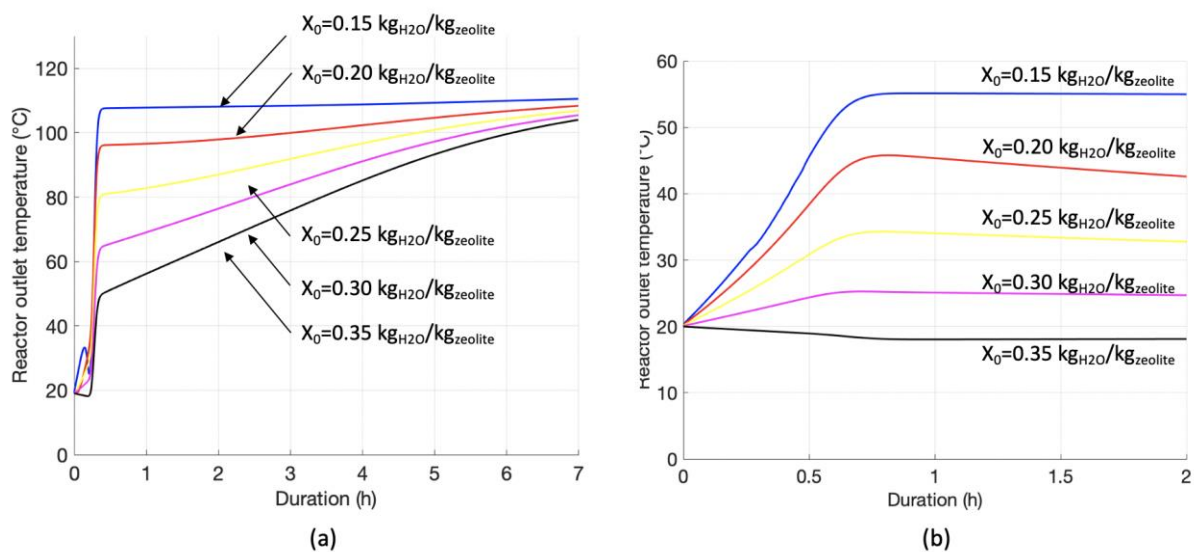


Figure 15 Influence of initial water uptake to the temperature profile in (a) charging and (b) discharging

5. Conclusions

The present study numerically investigates a three-phase thermochemical reactor. In the current literature, the development and numerical investigation of the three-phase reactor is necessary and meaningful. To address the current research gap in three-phase thermochemical reactors, according to the proposed three-phase reactor, the study demonstrates a numerical model to describe the heat and mass transfer. Within the reactor model, considerations have been made to the heat and mass conservation of the air, water and solid thermochemical material zeolite 13X. The software Matlab has been used to solve the equations and provide the evaluation of the heat and mass transfer. Original measurements obtained from the experimental tests are used to validate the numerical model. The good agreement between the computing value and experimental measurements are obtained through the 4 validation cases including charging and discharging tests. Followed by the validation, parameter sensitivity analysis is conducted with the highlight of the critical parameters to the numerical model output. The key outcomes of the study are summarised as follow.

- i. There is a fair agreement between the numerical and experimental values in the cases of charging and discharging with the root mean square percent error ranging from 6.02% to 12.29%.
- ii. Uncertainties in initial water content of zeolite and heat loss to the ambient lead to the discrepancy between the numerical and experimental values.
- iii. To increase water outlet temperature in discharging, control strategies should be investigated considering inlet air flow rate, inlet air temperature and water flow rate.
- iv. Reference diffusivity, heterogeneity factor, and initial water uptake can affect the numerical calculation results significantly. The application of the parameters should be adjusted to produce convincing computing values.
- v. The developed and validated three-phase thermochemical reactor model has provided fundamental basis for the reactor optimisation and performance evaluation.

6. Reference

- [1] Chenari B, Dias Carrilho J, Gameiro Da Silva M. Towards sustainable, energy-efficient and healthy ventilation strategies in buildings: A review. *Renew Sustain Energy Rev* 2016;59:1426–47. doi:10.1016/j.rser.2016.01.074.
- [2] Garg H, Mullick S, Bhargava V. *Solar thermal energy storage*. Berlin: Springer Science & Business Media; 2012.
- [3] Scapino L, Zondag HA, Van Bael J, Diriken J, Rindt CCM. Sorption heat storage for long-term low-temperature applications: A review on the advancements at material and prototype scale. *Appl Energy* 2017;190:920–48. doi:10.1016/j.apenergy.2016.12.148.
- [4] Aydin D, Casey SP, Riffat S. The latest advancements on thermochemical heat storage systems. *Renew Sustain Energy Rev* 2015;41:356–67. doi:10.1016/j.rser.2014.08.054.
- [5] Solé A, Martorell I, Cabeza LF. State of the art on gas-solid thermochemical energy storage systems and reactors for building applications. *Renew Sustain Energy Rev* 2015;47:386–98. doi:10.1016/j.rser.2015.03.077.
- [6] Michel B, Neveu P, Mazet N. Comparison of closed and open thermochemical processes, for long-term thermal energy storage applications. *Energy* 2014. doi:10.1016/j.energy.2014.05.097.
- [7] Tatsidjodoung P, Le Pierrès N, Heintz J, Lagre D, Luo L, Durier F. Experimental and numerical investigations of a zeolite 13X/water reactor for solar heat storage in buildings. *Energy Convers Manag* 2016;108:488–500. doi:10.1016/j.enconman.2015.11.011.
- [8] Kuznik F, Gondre D, Johannes K, Obrecht C, David D. Numerical modelling and investigations on a full-scale zeolite 13X open heat storage for buildings. *Renew Energy* 2019;132:761–72. doi:10.1016/j.renene.2018.07.118.
- [9] Gaeini M, Wind R, Donkers PAJ, Zondag HA, Rindt CCM. Development of a validated 2D model for flow, moisture and heat transport in a packed bed reactor using MRI experiment and a lab-scale reactor setup. *Int J Heat Mass Transf* 2017;113:1116–29. doi:10.1016/j.ijheatmasstransfer.2017.06.034.
- [10] Fopah-Lele A, Kuznik F, Osterland T, Ruck WKL. Thermal synthesis of a thermochemical heat storage with heat exchanger optimization 2016. doi:10.1016/j.applthermaleng.2015.12.103.

- [11] Schreiber H, Graf S, Lanzerath F, Bardow A. Adsorption thermal energy storage for cogeneration in industrial batch processes: Experiment, dynamic modeling and system analysis. *Appl Therm Eng* 2015;89:485–93. doi:10.1016/j.applthermaleng.2015.06.016.
- [12] Mohammadzadeh Kowsari M, Niazmand H, Tokarev MM. Bed configuration effects on the finned flat-tube adsorption heat exchanger performance: Numerical modeling and experimental validation. *Appl Energy* 2018;213:540–54. doi:10.1016/j.apenergy.2017.11.019.
- [13] De Boer R, Smeding SF, Zondag HA, Krol G, De Boer R, Smeding S, et al. Development of a prototype system for seasonal solar heat storage using an open sorption process 2014.
- [14] Mette B, Kerskes H, Drück H. Experimental and numerical investigations of different reactor concepts for thermochemical energy storage. *Energy Procedia* 2014;57:2380–9. doi:10.1016/j.egypro.2014.10.246.
- [15] Kuwahara F, Shiota M, Nakayama A. A numerical study of interfacial convective heat transfer coefficient in two-energy equation model for convection in porous media. *Int J Heat Mass Transf* 2001;44:1153–9. doi:10.1016/S0017-9310(00)00166-6.
- [16] R. Welty J, E. Wicks C, E. Wilson R, Rorrer G. Fundamentals of momentum, heat and mass transfer. vol. 13. 1970. doi:10.1016/0017-9310(70)90063-3.
- [17] Donald A. N, Adrian B. Convection in Porous Media. London: 2013.
- [18] Gondre D. Numerical modeling and analysis of heat and mass transfers in an adsorption heat storage tank: Influences of material properties , operating conditions and system design on storage performances 2017.
- [19] Hutson ND, Yang RT. Theoretical basis for the Dubinin-Radushkevitch (D-R) adsorption isotherm equation. *Adsorption* 1997;3:189–95. doi:10.1007/BF01650130.
- [20] Junzeng X, Qi W, Shizhang P, Yanmei Y. Error of Saturation Vapor Pressure Calculated by Different Formulas and Its Effect on Calculation of Reference Evapotranspiration in High Latitude Cold Region. *Procedia Eng* 2012;28:43–8. doi:10.1016/j.proeng.2012.01.680.
- [21] Mette B, Kerskes H, Drück H, Müller-Steinhagen H. Experimental and numerical investigations on the water vapor adsorption isotherms and kinetics of binderless zeolite 13X. *Int J Heat Mass Transf* 2014;71:555–61.

- doi:10.1016/j.ijheatmasstransfer.2013.12.061.
- [22] Trznadel BJ, Zietek S, Swiatkowski A. Validation of the Reliability of the Porous Structure Parameters for Activated Carbons as Evaluated on the Basis of Adsorption Isotherms from the Gaseous Phase. *Adsorpt Sci Technol* 1999;17:11–24.
- [23] A.W. Marczewski. Adsorption: Energetic Heterogeneity 2002. <http://adsorption.org/awm/ads/Het-src.htm#Het-type-energ> (accessed February 11, 2019).
- [24] Glueckauf E, Coates JI. 241. Theory of chromatography. Part IV. The influence of incomplete equilibrium on the front boundary of chromatograms and on the effectiveness of separation. *J Chem Soc* 1947:1315. doi:10.1039/jr9470001315.
- [25] Sircar S, Hufton JR. Why does the linear driving force model for adsorption kinetics work? *Adsorption* 2000;6:137–47. doi:10.1023/A:1008965317983.
- [26] Glueckauf E. Theory of chromatography: Part 10. - Formula for diffusion into spheres and their application to chromatography. *Trans Faraday Soc* 1955;51:1540–51. doi:10.1039/TF9555101540.
- [27] Kim H, Cho HJ, Narayanan S, Yang S, Furukawa H, Schiffres S, et al. Characterization of Adsorption Enthalpy of Novel Water-Stable Zeolites and Metal-Organic Frameworks. *Sci Rep* 2016;6:1–8. doi:10.1038/srep19097.
- [28] Daïan J-F. *Equilibrium and Transfer in Porous Media 2: Transfer Laws*. London: 2014.
- [29] Hengyi Chemical. Zibo Hengyi Chemical Science and Technology Co., Ltd 2018. https://zbhengyi.en.alibaba.com/productgroup/806185240/molecular_sieve.html?spm=a2700.icbuShop.74.2.67377be3uM8NoM (accessed February 26, 2019).
- [30] Sun LM, Ben Amar N, Meunier F. Numerical study on coupled heat and mass transfers in an absorber with external fluid heating. *Heat Recover Syst CHP* 1995;15:19–29. doi:10.1016/0890-4332(95)90034-9.
- [31] Sargent RG. Verification and validation of simulation models. *J Simul* 2013. doi:10.1057/jos.2012.20.
- [32] Shukla A, Tiwari GN, Sodha MS. Experimental study of effect of an inner thermal curtain in evaporative cooling system of a cascade greenhouse. *Sol Energy* 2008;82:61–72. doi:10.1016/j.solener.2007.04.003.
- [33] Allouche Y, Varga S, Bouden C, Oliveira AC. Validation of a CFD model for the

- simulation of heat transfer in a tubes-in-tank PCM storage unit. *Renew Energy* 2016. doi:10.1016/j.renene.2015.12.038.
- [34] Dolado P, Lazaro A, Marin JM, Zalba B. Characterization of melting and solidification in a real-scale PCM-air heat exchanger: Experimental results and empirical model. *Renew Energy* 2011. doi:10.1016/j.renene.2011.04.008.
- [35] Dubinin MM, Astakhov VA. Development of the concepts of volume filling of micropores in the adsorption of gases and vapors by microporous adsorbents. *Bull Acad Sci USSR Div Chem Sci* 1971;20:3–7. doi:10.1007/BF00849307.
- [36] Cortés FB, Chejne F, Carrasco-Marín F, Moreno-Castilla C, Pérez-Cadenas AF. Water adsorption on zeolite 13X: Comparison of the two methods based on mass spectrometry and thermogravimetry. *Adsorption* 2010;16:141–6. doi:10.1007/s10450-010-9206-5.
- [37] Gorbach A, Stegmaier M, Eigenberger G. Measurement and Modeling of Water Vapor Adsorption on Zeolite 4A—Equilibria and Kinetics. *Adsorption* 2004;10:29–46. doi:10.1023/B:ADSO.0000024033.60103.ff.